CONTROL CONCEPTS FOR AN AGILE AND HIGHLY SWEPT FLYING WING CONFIGURATION

P. Löchert
DLR, Institute of Aerodynamics and Flow Technology,
Lilienthalplatz 7, Braunschweig, D-38108

K.C. Huber
DNW, German-Dutch Wind Tunnels
Bunsenstraße 10, Göttingen, D-37073

M. Rütten
DLR, Institute of Aerodynamics and Flow Technology,
Bunsenstraße 10, Göttingen, D- 37073

Abstract

This paper presents results of current DLR research on the stability and control behavior of a generic flying wing configuration. The geometry considered here is a flying wing configuration with a leading edge sweep angle of 53°. The focus of the investigations is the controllability of such type of configuration without a vertical tail plane for yaw control to reduce the radar cross section. The configuration is characterized by a non-linear aerodynamic behavior with a complex vortical flow field. Therefore extensive experimental investigations on the influence and effectiveness on spoiler geometries on such type of configuration have been conducted as well as numerical investigation for different control concepts. Due to the vortical flow field a control device vortex interaction results and changes the aerodynamic behavior of flap based control devices. Besides more or less sophisticated flap based control devices a control concept using thrust vectoring to increase the maneuverability is considered as well. The results presented in this paper provide an important contribution for the design of future control concepts for controllability of highly swept flying wing configurations.

1. INTRODUCTION

Recent Unmanned Combat Air Vehicle (UCAV) configurations and design studies use medium to highly swept wings with round or variable leading edge (LE) geometries. The performance and signature considerations often result in medium leading edge sweep angles of 45° – 60°. The design constrains of future agile and low observable UCAV configurations are a compromise between a minimum cross section and an advanced flight performance to achieve long range with remaining agility.

The objectives of the paper are related to the internal DLR project Mephisto and have been set up in cooperation with the NATO STO[1] – AVT[2]-251 workgroup: aim of this workgroup is to perform a multi-disciplinary UCAV design, which resulted in the development of the MULDICON[3]. The challenge of the design is to achieve high agility and flight performance without a vertical tail plane for yaw control to reduce the radar cross section [1]. These types of configurations have a strong non-linear aerodynamic behavior and the flow dominated by complex vortex systems, including vortex-to-vortex and vortex-to-boundary layer interactions. For this reasons investigations on the influence and effectiveness of alterative control concepts for yaw controllability are necessary.

[1] Science and Technology Organization
[2] Applied Vehicle Technology
[3] MULti DIsciplinary CONfiguration

Due to the vortical flow field on the upper wing side for medium to high angle of attack (AoA) a control device vortex interaction occurs. In a previous study of Winkler et al. [2] the influence of the vortex dominated flow field on the effectiveness of unconventional spoiler geometries at the trailing edge (TE) is shown.

The present investigation analyses the effect of the aerodynamic behavior of different alternative yaw control devices. The boundary conditions of the required effectiveness of the control device result from the flight mechanical requirements acquired in the NATO STO AVT-251 research Task Group by Liersch et al. [3]. The summarized flight mechanical requirement for the presented studies is a necessary yawing moment c_n of at least $1.5 \cdot 10^{-2}$ with an almost neutral influence on rolling and pitching moment. To keep the radar cross section low the deflection and the size of the control surfaces is restricted and should be as small as possible. Regarding the necessary yawing moment a maximized lever arm for this type of control surface is favorable. For this reason flap based control concepts like spoiler and split flaps have been applied and assessed within in a design study for the MULDICON.

Additional a CFD study is presented within this paper which investigates different mechanical and fluidic thrust vectoring approaches. Tight requirements with regard to the infrared and radar signature are the reason why highly integrated engines, submerged air intakes and engine nozzles are preferred solutions for UCAVs. From the infra-

doi:10.25967/480010

red point of view the engine exhaust plume should possess an overall low temperature level and its characteristic temperature profile should be smeared over in a way that it cannot be recognized and assigned to an engine jet by any hostile anti-aircraft missile. Therefore, high-aspect ratio nozzles are used although they show deficits regarding the thrust level due to additional friction and redirection of flow.

As the strong demand for low observability poses an additional design constraint, unconventional control effectors such as mechanical and fluidic thrust vectoring devices gain more and more interest [5]. Existing solutions for fighter aircrafts cannot be used since they are made for rotationally symmetric or nearly quadratic nozzles. The challenge is to develop efficient thrust vectoring devices for high-aspect ratio nozzles under the aspect of low radar and infrared observability. This study concentrates on two different types of mechanical thrust vectoring devices, which are investigated in order to identify trends of the yaw control potential. Additional a fluidic thrust vectoring devices with different exhaust jet control possibilities is introduced.

First, the baseline configuration is presented in the following chapter. The subsequent chapter will draw out the experimental results of low speed wind tunnel tests for different spoiler configurations. Thereupon the numerical approach is described followed by the numerical results of the considered control concepts.

2. BASELINE CONFIGURATION

The baseline configuration in this report is the MULDICON planform with the geometrical dimensions as outlined in **Figure 1**. A more detailed description of the configuration can be found in Cummings et al. [6]. The planform is similar to the SACCON[4] but exhibits a TE sweep angle of $\varphi_{TE} = 30°$, whereas the airfoils remain like the ones of the SACCON. The SACCON was designed in a preceding NATO STO-AVT-161 Task Group to investigate the Stability and Control behavior of highly swept flying wing configuration and is described in Cummings and Schütte et al. [7]. For a better comparison between the moment coefficients, all moment coefficients are related to the same reference length $c_{ref} = 6m$.

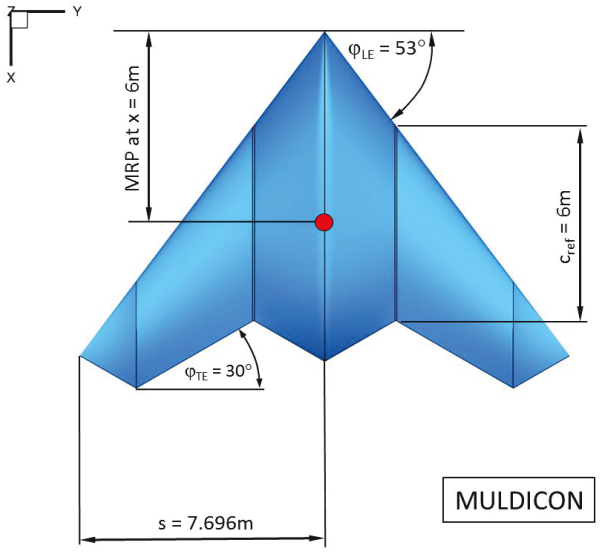

Figure 1 MULDICON Geometry

[4] Stability And Control CONfiguration

The considered flight condition in this report represent the condition for the approach case in the flight map with $M_\infty = 0.4$ at sea level and a Reynolds number of $Re_\infty = 55.9 \cdot 10^6$. Due to the similar planform, leading edge sweep angle and radius contour of the MULDICON and SACCON configuration the flow topology of both configurations are comparable for the same onflow conditions. For the SACCON the flow topology is described in Zimper et al. [8] and Cumming and Schütte et al. [7]. The resulting flow topology of the MULDICON for the here considered flight condition is presented in **Figure 2**. It shows the pressure coefficient and the skin friction lines for the baseline configuration of the MULDICON at an AoA of $\alpha = 8°$ and 12° from numerical investigations with RANS method DLR TAU. At an AoA of $\alpha = 8°$ a separation at the sharp leading edge apex has developed which becomes larger with increasing the AoA. Additional an integrating yaw control device at the wingtip is most affected by the tip vortex, which occurs at an AoA of $\alpha \approx 8°$ and its onset point moves towards the apex along the LE with increasing AoA.

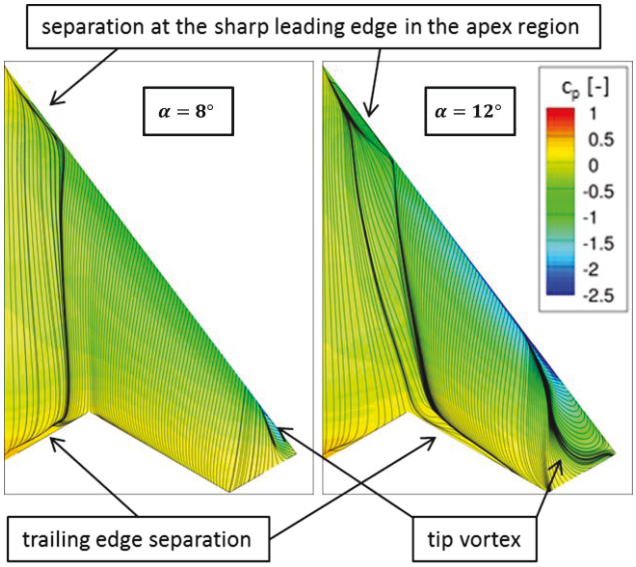

Figure 2 MULDICON Topology (Baseline, $M_\infty = 0.4$, $Re_\infty = 55.9 \cdot 10^6$)

3. EXPERIMENTAL RESULTS

Preceding experimental investigations conducted within the low-speed regime with the DLR-F19 wind tunnel model lead to the development of the spoiler concept of the MULDICON. These are presented within this chapter. The DLR-F19 wind tunnel model is based on the SACCON and accommodates control devices as described in Cummings and Schütte et al. [7]. The wind tunnel model was designed at the DLR Institute of Aerodynamics and Flow Technology, structurally dimensioned by Leichtwerk AG and was built at the DLR Braunschweig workshop.

The DLR-F19 model is dimensioned for static as well as dynamic testing, up to a maximum velocity of $V_\infty = 90 \frac{m}{s}$ ($M_\infty = 0.256$). The model has a weight of approximately 10kg and can be equipped with a wide range of different control surfaces along the TE as well as with spoiler geometries within the body region of the configurations upper side.

The model has been subject to a number of experimental test campaigns. Through the first three low speed wind tunnel experiments the effects of conventional trailing edge control surfaces have been studied in Huber et al.

[9]. Throughout the here presented experimental investigations the model has been equipped with non-conventional control surfaces, namely spoilers. The test has been conducted at Mach number of $M_\infty = 0.15$ within the low speed facility DNW[5]-NWB in Braunschweig.

Throughout the test campaign all tested spoiler configurations, apart from one, gave rise to coupled influences on all moment coefficients. This means that no isolated influence of the yawing moment coefficient from the others could be achieved. One spoiler configuration however was identified where only the yawing moment was influenced by the spoiler but not the pitching and rolling moment. For this the spoiler is located on the upper and lower side at the wingtip, deflected perpendicular to the flow with a deflection angle of $\delta_u = 90°$ on the upper and $\delta_l = 90°$ on the lower side. The experimental setup for this particular spoiler configuration for two different spoiler heights can be seen in **Figure 3**.

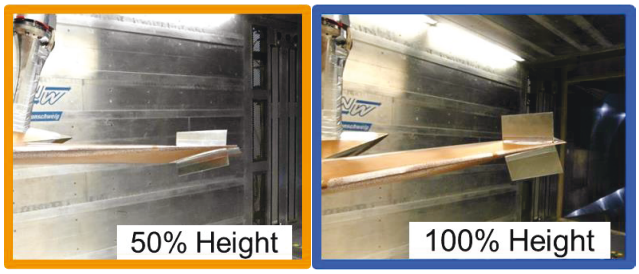

Figure 3 Experimental setup with a double sided spoiler on the wingtip

Figure 4 shows the resulting pitching moment development with AoA for the clean configuration and a spoiler setup with 50% and 100% height, the corresponding yawing moment development is plotted in **Figure 5**.

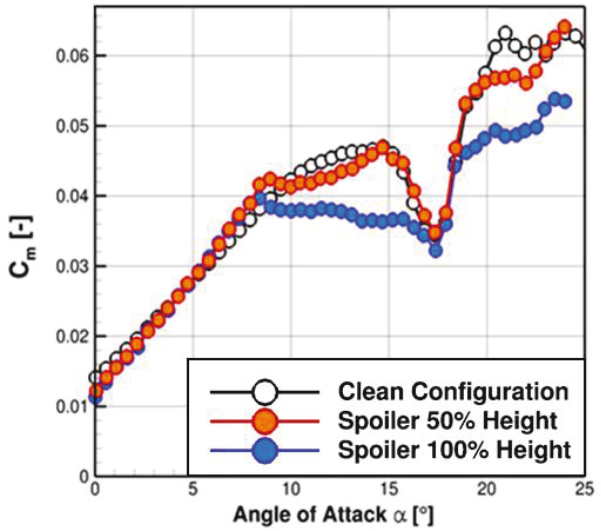

Figure 4 Pitching moment of the double sided spoiler at the wingtip ($M_\infty = 0.15$, $Re_\infty = 1.5 \cdot 10^6$, $\delta_u = 90°$ and $\delta_l = 90°$)

As it can be seen from Figure 4, the spoiler 100% Height configuration gives rise to a coupled set of coefficients for AoA $\alpha > 8°$. When however the height of the spoiler is reduced by 50% a sole influence in yaw, though also reduced in value, can be achieved up to an AoA of $\alpha = 10°$. Furthermore the control device offers a nearly constant yawing moment over the AoA up to $\alpha = 10°$. For higher AoA the influence on the yawing moment decreases and the differences in the pitching moment between the spoiler and the clean configuration increases. So a feasible controllability with this configuration at higher AoA is not given.

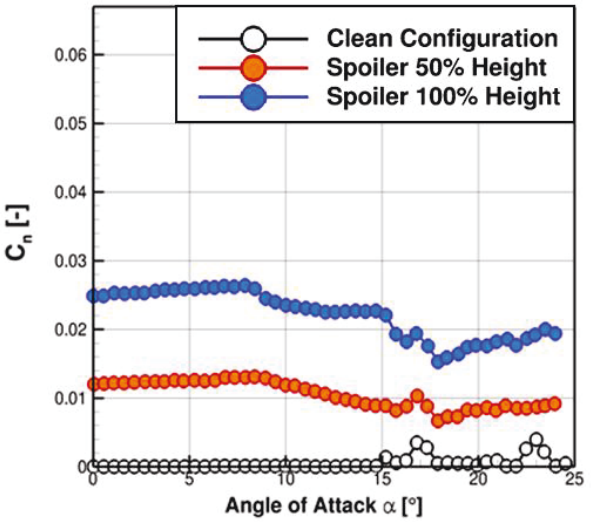

Figure 5 Yawing moment of the double sided spoiler at the wingtip ($M_\infty = 0.15$, $Re_\infty = 1.5 \cdot 10^6$, $\delta_u = 90°$ and $\delta_l = 90°$)

4. NUMERICAL APPROACH

In this chapter the general descriptions of the flow solver TAU and the applied computational grids for this study are presented.

4.1. DLR Flow Solver TAU

Within the present study the DLR flow solver TAU was used solving the compressible, three-dimensional RANS[6] equations. The DLR flow solver TAU is being developed by the DLR Institute of Aerodynamics and Flow Technology [10]. The solver is based on a finite volume formulation. For the here conducted simulation a cell vertex metric is used in combination with a multigrid approach. DLR TAU can be applied on unstructured hybrid grids which allow working with different types of elements. Prismatic elements are used to resolve the viscous shear layers close to the walls, whereas the remaining field is resolved with tetrahedral elements.

For the presented simulations the one-equation Spalart-Allmaras (SA) turbulence model in its negative form (SA-neg) is used. The SA-neg formulation is less sensitive to particularly negative values of the transport turbulence quantities [11].

4.2. Computational Grids

The hybrid unstructured grids applied for the simulations have been generated with the hybrid grid generator Centaur, developed by CentaurSoft [12]. For all hybrid grids the initial layer thickness of the first prismatic layer is 0.005mm, resulting in a typical y+ value of approximately one. The boundary layer is fully resolved using 30 prismatic layers. Over the entire surface of the configuration the full 30 prismatic layers can be achieved, hence no chopping of prismatic layers occurs. The hybrid unstructured grid can be seen in **Figure 6** with the surface in turquoise, the prismatic layers in red and a tetrahedral field grid in green. In **Figure 7** an enlarged viewing for the surface triangulation and the prismatic layers is shown.

[5] German-Dutch Wind Tunnels

[6] Reynolds-Averaged Navier-Stokes

Additionally, a special grid refinement at the leading edge and in the field close to the surface is applied to resolve the flow separation at the leading edge accurately and the vortical flow field respectively.

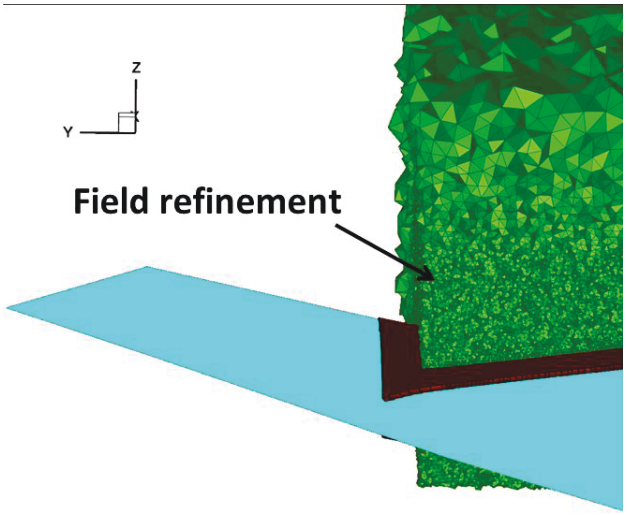

Figure 6 Tetrahedral field grid

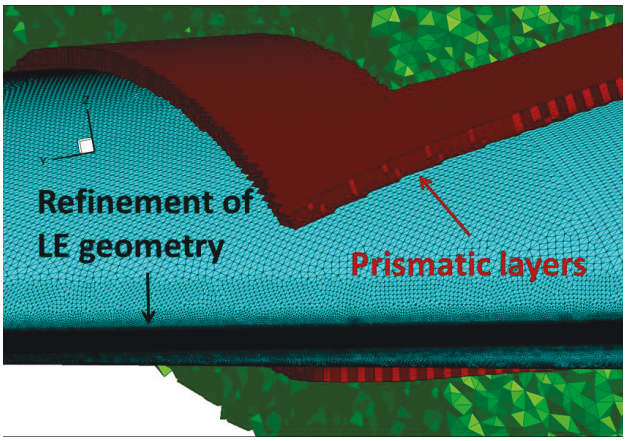

Figure 7 Prismatic layer and surface resolution

For the integration of the control device at the wingtip a modular grid approach was used. Hereby the grid around the configuration is divided into a main grid and a sub-grid. The main grid remains the same for all simulations and only a part of the geometry within a predefined bounding box (module) is being remeshed (sub-grid). Using this approach the time for the mesh generation can be significantly decreased. In the here presented case the module is placed around the wingtip and its panels are defined as interface panels to the main grid, hence any control device configuration located within the module at the wingtip can be meshed. First the main grid is generated, after the main grid generation the geometry within the module can be exchanged and only the grid within the module is being newly generated. The nodes on every interface panel from the main grid to the module are fixed and are used for the modular grid generation. This guarantees a continuous connection of both, the main grid and the sub-grid. This approach also allows for resolution of the LE which remains constant with spoiler geometry change; by this means the leading edge always triggers the same vortical flow field along the LE. With this strong similarity between all used grids a high comparability between the different grids can be achieved, which resulting in similar spatial discretization errors. The overall grid sizes amount to approximately 61 million nodes for a full model setup. The present numerical approach is validated for the SACCON with control devices and documented by Liersch et al. [1] and Schütte et al. [13].

5. NUMERICAL RESULTS

The numerical results for the control concepts are described in this chapter. First, the flap based control concepts are considered followed by an evaluation of a control concept using thrust vectoring.

5.1. Flap Based Control Concepts

A possible control concept with a wingtip flap is described in Paul et al. [14] for the SACCON and Loechert et al. [15] for the MULDICON; here the wingtip was deflected in an asymmetric way to convert the lift force into a side force. However the overall controllability of this control concept was not sufficient to fulfill the requirements.

Based on the experimental investigation with the DLR-F19, it was found that spoiler deflected perpendicular to the flow at the wingtip will solely have an effect on the yawing moment. Loechert et al. [15] presented a possible control concept, similar to the aforementioned one, for the MULDICON. This subchapter shows the numerical results of studies which focused on spoilers and a similar type of control device; a split flap located at the wingtip of the MULDICON.

For comparison purposes differences between the moment coefficients of the configuration with flap based control devices and the baseline clean configuration $\Delta C_{l,m,n} = C_{l,m,n}$(with control device) - $C_{l,m,n}$(clean) is used in this subchapter.

5.1.1. Spoiler

In the following section a study with similar spoiler geometry like those applied to the DLR-F19 configuration have been assessed. Similar to the experimental investigations the spoiler is also located on the upper and the lower side of the wingtip but is applied to the MULDICON. The MULDICON with integrated spoilers for yaw control can be seen in **Figure 8**.

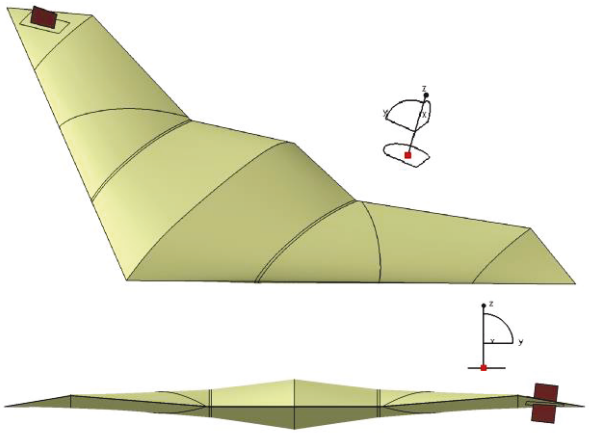

Figure 8 MULDICON with integrated spoiler deflected perpendicular to the flow (δ_u = 90° and δ_l = 90°)

As in the wind tunnel test the spoilers are deflected perpendicular to the flow with a deflection angle of δ_u = 90° on the upper and δ_l = 90° on the lower side.

Within the study the influence of the positioning of the

spoiler on the wingtip, in specific the relative distance of the spoiler between the LE and the TE was analyzed. Therefore the parameter "*rf*" is defined as the relative distance between the LE and TE, where *rf* = 0 is the position at the LE and *rf* = 1 the position at the TE. Three different positions of the spoiler were chosen. The relative distance *rf* of these positions are *rf* = 0.5, *rf* = 0.6 and *rf* = 0.75. The deflection angle on both sides is the same for all positions. For all relative positions the changes of the moment coefficients in comparison to the clean configuration are plotted versus the AoA in **Figure 9**. With increasing the relative position the gradients $\frac{\partial \Delta c_{l,m}}{\partial \alpha}$ decrease as well as the maxima of the rolling and pitching moment.

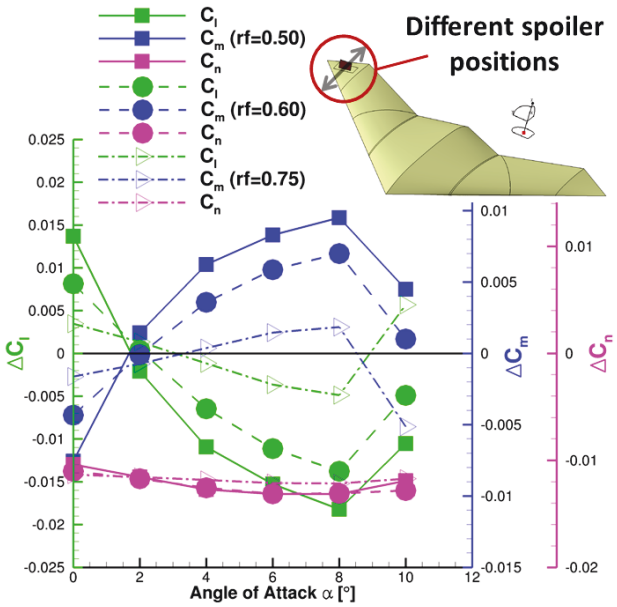

Figure 9 Moments distribution for different spoiler positions (M_∞ =0.4, $Re_\infty = 55.9 \cdot 10^6$, $\delta_u = 90°$ and $\delta_l = 90°$)

There are almost no changes in the yawing moment with changing the relative position. By changing the relative position from *rf* = 0.5 to *rf* = 0.75 the pitching moment is reduced by approximately 80% and the rolling moment by 75%. This means that the spoiler position should be as near as possible moved towards the TE to decrease the effect on the rolling and pitching moment sufficiently.

For a better understanding the pressure coefficient through the spoiler along the chord for all spoiler positions are plotted in **Figure 10**.

Due to the spoiler the lift on the wingtip is reduced in front of it. By increasing the relative distance *rf* the loss in lift is reduced. In the rear section of the spoiler a zone with negative lift exists and by increasing the relative distance *rf* the negative lift is reduced due to the smaller rear section.

Nevertheless, with the closest position of the spoiler to the TE a rear section with negative lift still exist. The total lift loss at the wing of the spoiler side causes a rolling moment. Reducing the lift loss means reducing the rolling moment. In addition the negative lift in the rear section causes a pitch up effect which can be seen in **Figure 9** represented by the positive change of the pitching moment. To minimize such pitch up effect, a configuration without a rear section is required. This tends to the configuration with a split flap where no rear section of the wing exists.

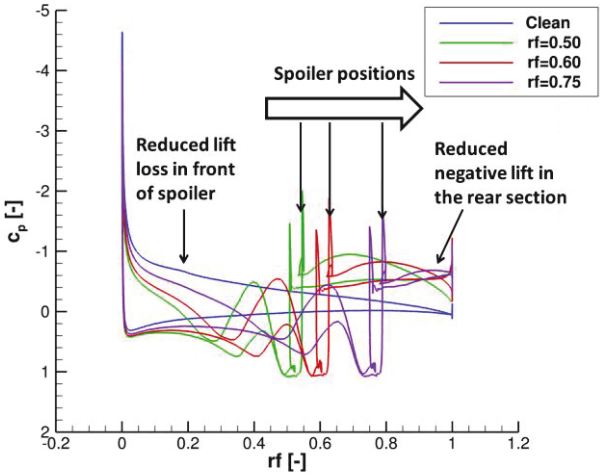

Figure 10 C_P distribution through the spoiler along the chord (M_∞ =0.4, $Re_\infty = 55.9 \cdot 10^6$, $\delta_u = 90°$ and $\delta_l = 90°$)

Before the control concept with the split flap is presented the flow topology with the spoiler should be discussed. In **Figure 9** it has been shown that a drop of the pitching moment from α = 8° to α = 10° is going along with an increase in rolling moment. The influences presented in this chapter are more or less only applicable for attached flow conditions. However, at higher AoA the flow topology changes. **Figure 11** visualizes the change of the flow topology with spoiler between the AoA of α = 8° and α = 10°. For α = 8° the tip vortex and the wake flow of the spoiler are separated. By increasing the AoA to α = 10° the tip vortex interacts with the spoiler and with the wake flow of the spoiler. This interaction will be called in the following as “control device vortex interaction”. In comparison to α = 8° the control device vortex interaction at α = 10° causes a change of the pressure distribution and a change of the moment coefficients. This causes the drop in pitching moment and an increase of the rolling moment as plotted in **Figure 9**.

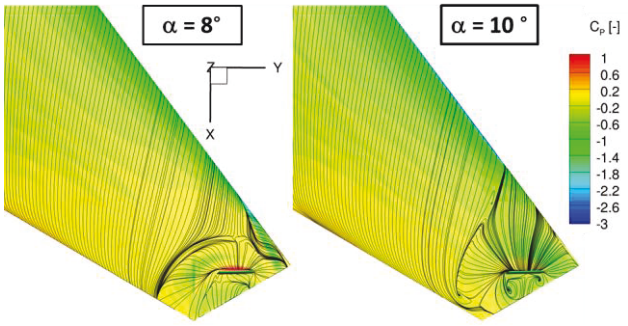

Figure 11 Comparison of the flow topology (M_∞ =0.4, $Re_\infty = 55.9 \cdot 10^6$, $\delta_u = 90°$ and $\delta_l = 90°$)

5.1.2. Split Flap

Based on the conclusion regarding the spoiler investigations a split flap might be a promising concept for effective yaw controllability. Therefor a double sided split flap was designed for the wingtip. For the deflection of the split flap a first estimation with empirical data was done. The deflection angles of $\delta_u = 45°$ for the upper split flap and $\delta_l = 32°$ for the lower split flap were kept constant. The designed split flap for MULDICON is shown in **Figure 12** with the double sided split flap in purple.

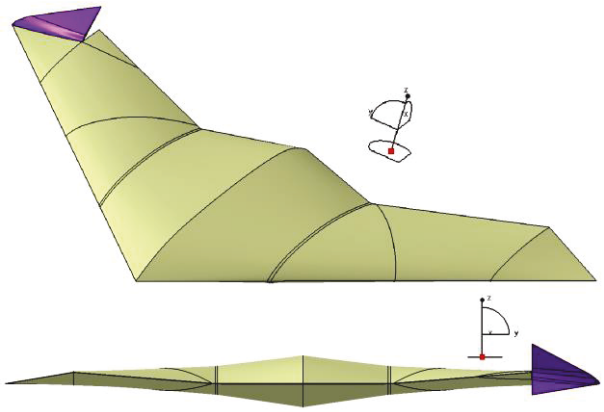

Figure 12 MULDICON with split flap ($\delta_u = 45°$ and $\delta_l = 32°$)

To analyze the effect of the vortical flow field on the control devices, CFD simulations with higher AoA and with different angle of sideslips (AoS) were performed with the TAU flow solver. The influence of the AoS on the yaw control device is quite crucial for the landing case. For the de-crab maneuver the yaw controllability must be guaranteed under crosswind condition.

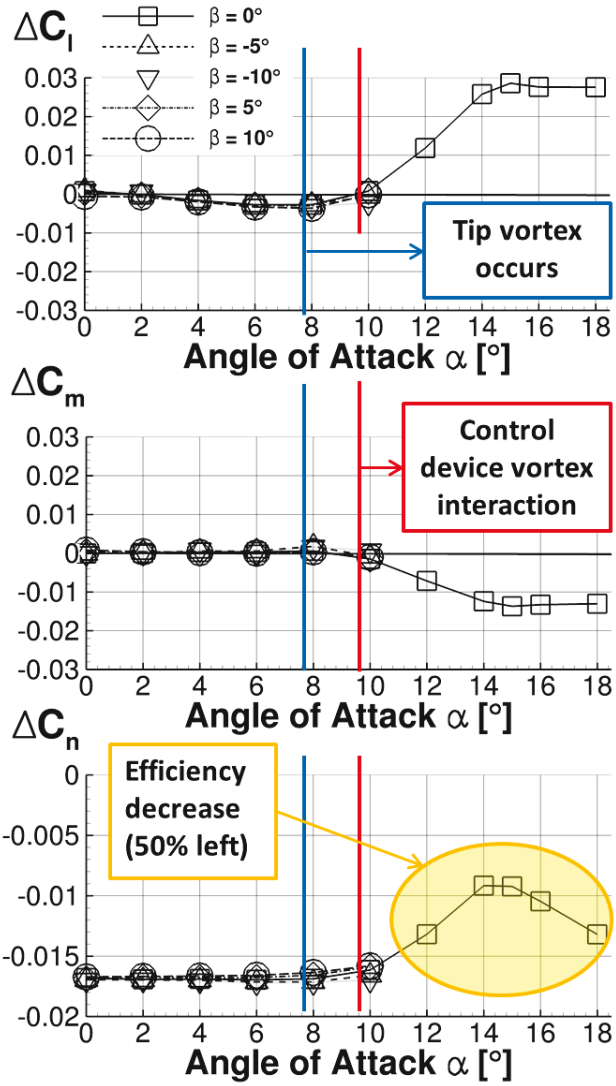

Figure 13 Moments distribution for the split flap with different angle of sideslips ($M_\infty = 0.4$, $Re_\infty = 55.9 \cdot 10^6$, $\delta_u = 45°$ and $\delta_l = 32°$)

In **Figure 13** the differences of the moment coefficients for the split flap in comparison to the clean configuration versus AoA for different AoS are plotted. First of all a feasible yawing moment of $C_n \approx -0.016$ with ΔC_l and $\Delta C_m \approx 0$ could be achieved for attached flow conditions. These conditions apply up to an AoA of $\alpha = 10°$ and an AoS of $\beta = \pm 10°$. Therefor the rolling, pitching and yawing moments are nearly constant versus AoA and AoS. For higher AoA like $\alpha = 10°$ the differences in rolling and pitching moment increase. In addition the yawing moment coefficient decreases. At an AoA of $\alpha = 14°$ the difference in rolling moment is three times higher and the pitching moment is two times higher than the generated yawing moment. The decrease in the efficiency results from the tip vortex. As marked in the **Figure 13** the tip vortex occurs on the upper wing side at an AoA of $\alpha \approx 8°$ and is getting larger with increasing AoA. At the same time its onset point moves along the LE towards the apex. At an AoA of approx. $\alpha \approx 10°$ the tip vortex interacts with the control device and the interaction increases with higher AoA.

In **Figure 14** and **Figure 15** the control device vortex interaction is visualized. In **Figure 14** the flow topology at an AoA of $\alpha = 10°$ is shown. The tip vortex is interfering with the control device at the outer corner, so the upper split flap is slightly affected by the tip vortex. At a higher AoA of $\alpha = 15°$ (**Figure 15**) the much larger tip vortex affects the entire split flap on the upper side of the wing. Furthermore the differences of the total pressure between the split flap side and the clean wing side in the wake flow decreases from the AoA of $\alpha = 10°$ to $\alpha = 15°$. This causes the decrease of the yawing moment.

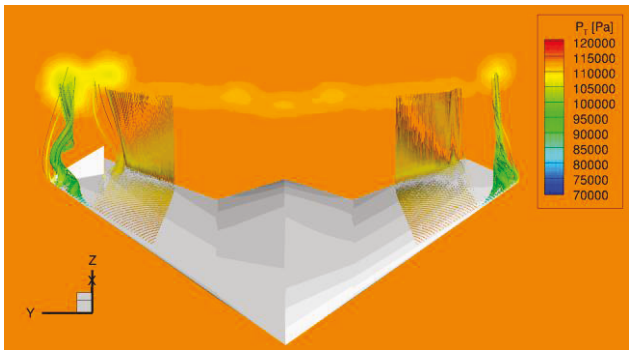

Figure 14 Control device vortex interaction ($M_\infty = 0.4$, $Re_\infty = 55.9 \cdot 10^6$, $\delta_u = 45°$, $\delta_l = 32°$ and $\alpha = 10°$)

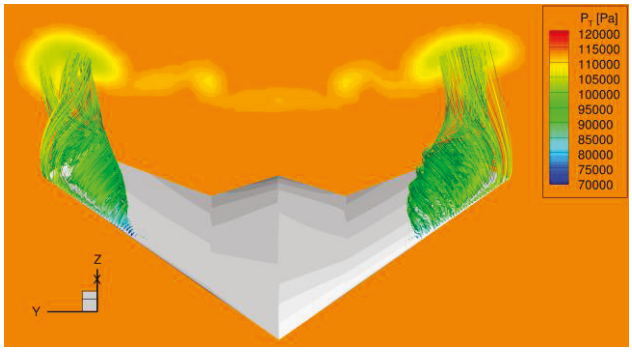

Figure 15 Control device vortex interaction ($M_\infty = 0.4$, $Re_\infty = 55.9 \cdot 10^6$, $\delta_u = 45°$, $\delta_l = 32°$ and $\alpha = 15°$)

5.2. Thrust Vectoring

Lower the detectability of a UCAV by dispensing the rudder has the negative effect of losing a very efficient control device in regard to yaw. This can partially retrieved by

using additionally integrated spoiler or split flaps accepting that parasitic effects on roll and pitch moments have to be balanced by other aerodynamic effectors. This contradicts the idea of being less detectable without a side rudder. Thus, an effective but low observable yaw control device is needed. Thrust vectoring is one possible solution, since it delivers an additional control possibility, which can offer benefits in terms of maneuverability and control effectiveness see Deere [16]. Moreover, it can also be a valuable control effector at flight situations with low dynamic pressures, where traditional aerodynamic control devices are losing efficiency. Additionally, thrust vectoring can be used to increase trim abilities of the aircraft and, thus, can finally reduce cruise trim drag. Last point is an important reason why such control devices are also important for low observable UCAV configurations as Mansion remarked [17].

In principle there are two approaches for achieving thrust vectoring: the mechanical and the fluidic control of the engine exhaust jet direction.

Mechanical thrust vectoring means deflecting the engine nozzle or parts of it and, therewith, mechanically redirecting the engine exhaust jet [18]. The mechanical thrust vectoring system is effective, however, it is heavy, complex in regard to actuator parts, and difficult to integrate, but easy to operate. From the infrared signature point of view the additional heating up of nozzle sections or mechanical parts is critical and has to be evaluated especially in regard to the detection probability. There are different types of mechanical thrust vectoring devices. In most cases the nozzle is either swiveled or reflector panels are used. These solutions are preferred in case of sonic engine exhaust jet flows of fighter aircraft as Wilde referred [19]. If the temperature of the hot engine exhaust jet is low enough and if the flow is shock free, then slewable thruster elements or guiding vanes are used.

The fluidic thrust vectoring is based on the idea to inject or remove fluid into or from the boundary of the primary jet flow to redirect the flow. In contrast to mechanical thrust vectoring devices the fluidic thrust vectoring systems have the advantage of being lightweight, simpler to integrate and free from thermally loaded moving parts, see Anderson [20]. Since thermal loads are critical in regard to infrared signature, it can be stated that fluidic systems shall reveal a lower aircraft observability penalty, in particular when the injection of hot gas flow is avoided, as Balu stated [21]. Research work is concentrating on shock thrust vectoring, or co-flow and counter-flow exhaust jet flow control, see Deere [22], thereto secondary jet or suction flows are used.

There is a significant difference regarding the counter-flow and co-flow concepts. Counter-flow concepts are based on the idea to locally reduce the momentum of the jet flow to be controlled, whereas in the co-flow case a secondary jet injects additional momentum to control the targeted jet flow. Besides the secondary jet or suction flows the Coanda effect is also used to facilitate or increase thrust vectoring, see Panitz [23]. Different studies investigated the counter-flow technique, in which Coanda surfaces were positioned at the exit of the primary jet, see Van der Veer [24]. Experiments were carried out for various nozzle shapes addressing the Coanda effect. It was found that a high thrust vector force can be achieved with relatively low secondary blowing or suction rates, when the primary jet is forced to attach itself to the Coanda surface, as Flamm showed [25].

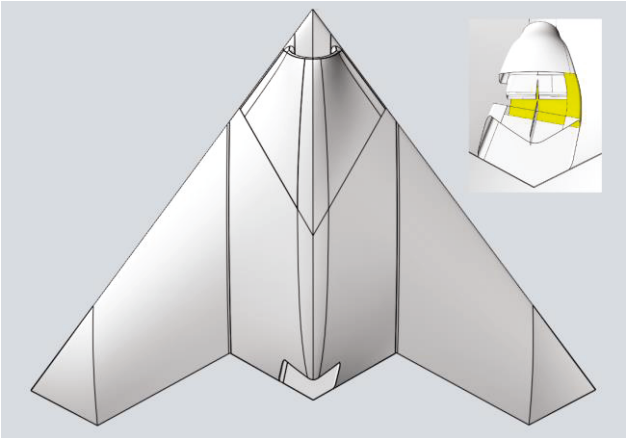

Figure 16 CAD drawing of the slewable mechanical nozzle, integrated in MULDICON, deflection angle (15°)

Low observability is a key element for the survivability of air vehicles without superior agility such as the MULDICON. Therefore, the internal integration of systems in a very flat vehicle planforms is an essential design requirement. Of course a consequence of such design concept is also the high aspect ratio of the nozzle. This had to be addressed by the design of the mechanical thrust vectoring device. The outcome of the design is depicted in the CAD drawing in **Figure 16**. The image shows a top view on the MULDICON with its integrated slewable nozzle. The cut-out section of the nozzle is visible at the rear part of the fuselage. The internal hot jet core shrouding with its two-sectional vent is also depicted in the mini-figure at the top right of the image. One specialty is the internal cold air splitting device which reduces the infrared detectability.

The second configuration is a slight variation of the first simple slewable nozzle: At the slewed nozzle middle segment a guiding vane respectively a jet rudder is additionally mounted to enforce the thrust vectoring efficiency. This flow actuation element is not curved, despite a well curved flow guiding vane would be a better solution. Here, only a technically feasible solution was investigated and no optimization had been performed. The geometrical deflection angle of the swiveled nozzle and the jet rudder (if mounted) is 15°. Then, the inner nozzle side wall has a curvature with a radius of roughly 3190 mm, the outer wall curvature radius is 3271 mm. To realize such a geometrical deformation is challenging, it might be necessary to develop new shape morphing concepts, materials and technologies. However, this effort might be worthwhile, in particular, when, under the special aspect of detectability, the potential for thrust vectoring is high enough.

The design of a fluidic thrust vectoring device has to take into account different flow phenomena which are essential for the redirection of the engine exhaust flow. Basically momentum has to be transferred to or away from the primary jet flow coming out of the engine. As discussed above the targeted jet flow deflection can be realized by blowing, suction or increasing shear. In the present work the design idea was the following: instead of using only one jet or suction control or other manipulation device the objective of the engineering work was to develop an efficient combination of secondary jet and suction control devices adapted to a specific nozzle shape, which could be integrated in a UCAV configuration.

The CAD adaptation of this concept is shown in **Figure 17**. It is obvious that the rear part of the UCAV had to be changed significantly: the upper nozzle cut out sections

had been closed and the Coanda surface had been increased by thickening the fuselage at the nozzle section. Bearing in mind the objective to concentrate on the efficiency of thrust vectoring the decision was made to simplify the nozzle section in order to reduce the computational effort. The details of the simplified nozzle design and the assignment of boundary conditions for two Mach number flow cases, $M_\infty = 0.48$ and $M_\infty = 0.8$, are shown in **Figure 18**.

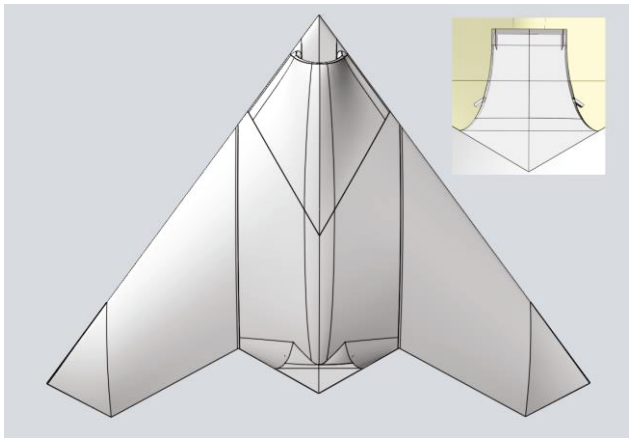

Figure 17 CAD drawing of the fluidic thrust vector nozzle, integrated in MULDICON

The pressure data shown for the simulation setup are also an outcome of the engine design of the DLR engine design group, whereas the pressure data of jet actuation devices are an outcome of the present simulation study.

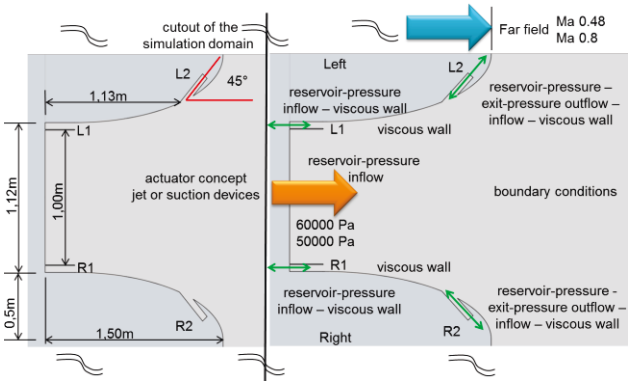

Figure 18 Assignment of the jet actuators of the fluid thrust vector nozzle and the boundary conditions for CFD simulation

Now, the CFD simulation results for the mechanical and fluidic vectoring devices configurations are discussed next, only the $M_\infty = 0.8$ results are shown.

In **Figure 19** the flow field of the $M_\infty = 0.8$ with the swiveled nozzle is shown, the temperature distribution on a cut-plane indicates a significant thrust vectoring capability. The analysis concentrates on the deflected engine exhaust jet flow observed from a rear point of view On the left side of the nozzle the flow separates earlier, thus the deflection angle does not keep the 15°, it has round about 12°, on the right the 15° is enforced. The same can be observed in **Figure 20**, the jet rudder increases the vectoring effect slightly, which is indicated by the cold air coming from the special internal splitting device and flowing around the jet rudder. Here the flow on the left side achieves a deflection angle of 13°.

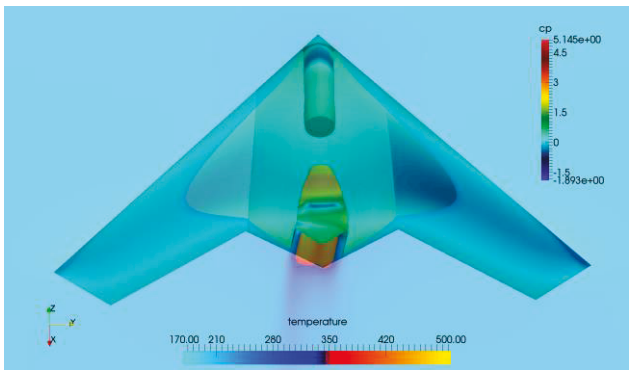

Figure 19 Flow field of the mechanical thrust vectoring case without additional jet rudder, visualized by the temperature distribution on a cut -plane, Cp values on MULDICON ($M_\infty = 0.8$ and $Re_\infty = 36 \cdot 10^6$)

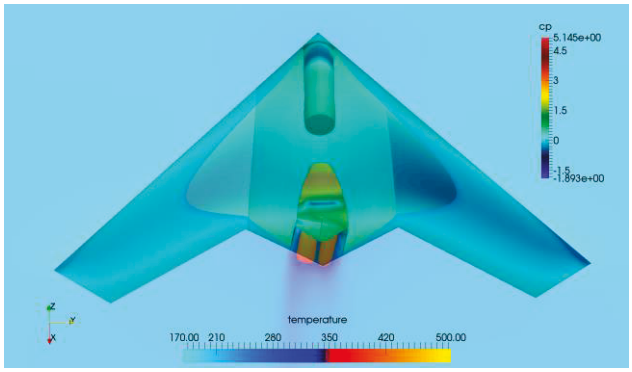

Figure 20 Flow field of the mechanical thrust vectoring case with additionally mounted jet rudder, visualized by the temperature distribution on a cut-plane, C_P values on MULDICON ($M_\infty = 0.8$ and $Re_\infty = 36 \cdot 10^6$)

Now, the CFD results of the fluid thrust vectoring device are analyzed. Again the two Mach number flow cases, $M_\infty = 0.48$ and $M_\infty = 0.8$, are investigated. For each two fluidic actuation cases are examined: the so called ``JR2'' and ``SL2 JR1 JR2'' cases. In the first case only the jet flow (J) is activated at the position 2 on the right side (R) of the nozzle and is visualized in **Figure 21**. The second fluidic actuation case in **Figure 22** is more complex, here both jets on the right are activated whilst on the left (L) at position 2 the suction (S) is activated.

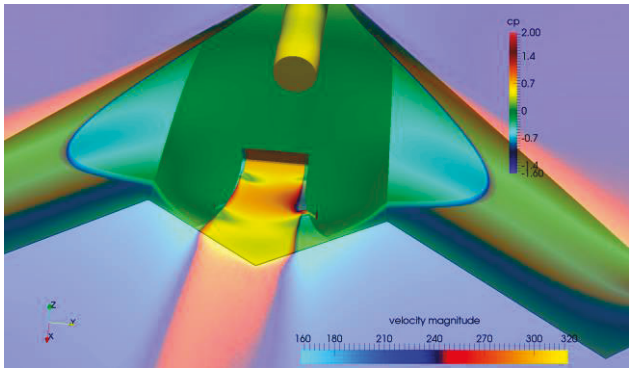

Figure 21 Flow field of fluidic thrust vectoring case JR2, visualized by velocity magnitude on the cut plane, C_P values on MULDICON ($M_\infty = 0.8$ and $Re_\infty = 36 \cdot 10^6$)

In both cases the fluidic actuation is able to deflect the engine exhaust jet by a relevant deflection angle of nearly 9.5°. Again the flow topologies reveal barely visible differences: in the case of the additionally inflowing jet at position 1 on the right. The exhaust jet is a little bit broader,

and the upstream effect of the jet actuator at position 2 is smaller. However, the nozzle-flow similarity of both actuation cases is a clear indication that the most effective actuator is the counter and cross flow acting jet at position 2. Suction and additional inflow are only enforcing the global effect.

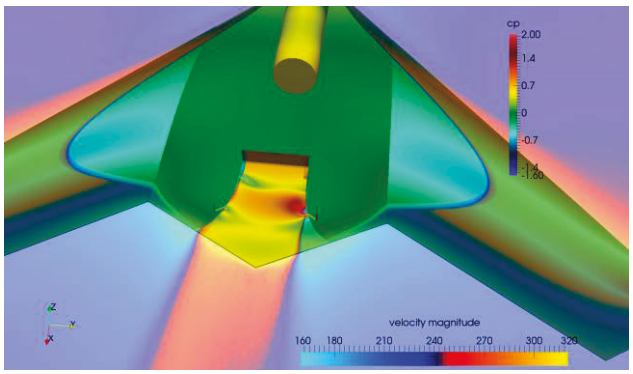

Figure 22 Flow field of fluidic thrust vectoring case SL2 JR1 JR2, visualized by velocity magnitude on the cut plane, C_P values on MULDICON ($M_\infty = 0.8$ and $Re_\infty = 36 \cdot 10^6$)

The flow structures of the nozzle flow are the same as in the $M_\infty = 0.48$ cases but the engine exhaust jet is slightly more bundled. The flow separation on the left occurs a little bit later, and the deflection angle is slightly higher with 11°. Again, it has to be emphasized that in this study the focal point was the applicability of such fluidic devices not their optimization, hence, the essential statement is, that the fluidic actuation is also working for transonic flows.

Based on the CFD results an assessment of the competing thrust vectoring devices has been conducted. For the evaluation the deflection angles and the yawing moment coefficients have been taken into account for the flow and actuation type scenarios discussed above. Again, it has to be remarked that the Mach number flow cases $M_\infty = 0.48$ and $M_\infty = 0.8$ are using engine data from different flight mission scenarios, hence, a comparison between these Mach number flow cases is limited, hence, only qualitative statements can be issued. However, the results for the same Mach number flow cases but different actuation types can be quantitatively assessed.

Thrust vectoring type	Mach number	Jet deflection [°]	C_n
mechanical bypass	0.48	12-15	0.03508
mechanical bypass + jet rudder	0.48	13-15	0.03542
mechanical bypass	0.8	12-15	0.02305
mechanical bypass + jet rudder	0.8	13-15	0.02408
fluidic actuation “JR2”	0.48	9.0	0.02837
fluidic actuation “SL2 JR1 JR2”	0.48	9.5	0.03404
fluidic actuation “JR2”	0.8	10.5	0.02461
fluidic actuation “SL2 JR1 JR2”	0.8	11.0	0.03436

Table 1 Efficiency of the investigated thrust vector devices

An overview over the three resulting evaluation quantities is given in **Table 1**. It is obvious that in the case of the fluidic thrust vectoring jet, deflection angles up to 11°, which can be achieved without further optimization, are lower than those achievable deflection angles of 15° enforced by the mechanical thrust vectoring. The aspect ratio of the nozzle and the resulting flatness of the exhaust jet are the explanation for the lower deflection angle. Even the counter-cross flow jet actuator cannot affect the exhaust jet over its whole width. The separation of the exhaust jet on the opposing part wall is more or less localized by the shape of the curved Coanda surface. This limits the average deflection angle. Nevertheless, the results are in that specific range which make such type of devices interesting for controlling the yawing moment, in particular, when bearing in mind that optimization procedures would be able to exploit further potential of this thrust vectoring technology.

The resulting values in **Table 1** reveal that the mechanical devices are working more efficient at lower Mach number flow cases. This might be a result of the special mission conditions which are defining the engine boundary conditions. A further parametric study is necessary to clarify this point. Besides, it is obvious that the combination of a curved bypass shroud with a suitable jet rudder shows best results. The jet rudder itself is not curved, this provides huge potential for further optimization. Interestingly, the fluidic thrust vectoring shows good actuation results for both Mach number flow cases, although the engine boundary conditions are nearly the same. The reason for that might be the adaptation of the control jet to the main engine exhaust jet conditions whilst the mechanical device has a fixed shape which is not adapted to the changed engine exhaust flow condition. However, to clarify this point further studies are needed.

6. CONCLUSION

In the present paper three different control concepts for yaw controllability are considered. The study is based on preliminary investigations carried out in experiments with spoilers applied to the DLR-F19 and numerical validations of different control devices applied to the MULDICON using the DLR RANS solver TAU. The experimental results show that a double sided spoiler positioned at the outer wing region generates an uncoupled yawing moment. The numerical results of the spoilers confirm that a position of the spoiler close to the trailing edge improves the behavior of such control device. However a control device vortex interaction occurs for higher AoA which decreases the efficiency of the upper spoiler and split flap respectively. The control device vortex interaction changes the aerodynamic topology and influences the moment coefficients. Spoilers and split flaps located close to the TE at the wingtip area are less sensitive regarding small AoA but the sensitivity increases for higher AoA.

Nevertheless a split flap is a feasible control device for yaw authority. For landing, AoA between $\alpha = 5°$ and $\alpha = 10°$ can be estimated with a Mach number smaller than the one considered here. The occurrence of the tip vortex depends on the flight condition as well as on the aerodynamic shape design. In the present study the control device vortex interaction occurs around an AoA of $\alpha = 10°$, which means that the range of AoA is covered by the split flap where no interaction occurs. For smaller Mach numbers the occurrence of the tip vortex is shifted to higher AoA. To delay the interaction to higher AoA the design or

the location of the split flap can be change. Contrariwise moving the split flap closer to the inner wing region decreases the efficiency because of the reduced lever arm and increases the influence of the split flap or spoiler on the rolling and pitching moments.

It was also shown that both, the mechanical and the fluidic thrust vector control, achieved a high enough yaw control efficiency, although the devices are not optimized, which shows the potential of this concept and makes it valuable for further investigations. Due to the vortex interaction a flap based control concept on the outer wing region is inefficient for vortical flow, which occurs for smaller AoA at higher Mach numbers. On the one hand a thrust vector control device provides sufficient yaw control for lower as well as for higher Mach numbers, but on the other hand the controllability depends on the engine thrust level, which is for the landing case approach idle. So, a control concept with the combination of a flap based control device and thrust vectoring may a feasible control concept which covers the whole flight mission.

Therefor the results presented in this paper provide an important contribution for the applicability of different control devices and for the design of future control concepts for yaw controllability of highly swept flying wing configurations.

REFERENCES

[1] Liersch, C.M., Huber, K.C., Schütte, A., Zimper, D., Siggel, M. Multidisciplinary design and aerodynamic assessment of an agile and highly swept aircraft configuration. CEAS Aeronautical Journal, Volume 7, No. 4, pp. 677–694, Oct. 2016.

[2] Winkler, M.; Huber, K.: Numerische Bewertung innovativer Steuerflächen einer generischen Lambdaflügel-konfiguration. EB 124-2016/901, 2016.

[3] Carsten M. Liersch and Gavin Bishop. "Conceptual Design of a 53deg Swept Flying Wing UCAV Configuration", 2018 Applied Aerodynamics Conference, AIAA AVIATION Forum, (AIAA 2018-2839) https://doi.org/10.2514/6.2018-2839

[4] Huber, K.C.; Schütte, A.; Martin Rein, M.; Löser, T.: Experimental aerodynamic assessment and evaluation of an agile highly swept aircraft configuration. CEAS Aeronautical Journal, Oct. 2016. doi: http://dx.doi.org/10.1007/s13272-016-0219-y

[5] Mason, M. and Crowther, W., \Fluidic Thrust Vectoring for Low Observable Air Vehicles", 2nd AIAA Flow Control Conference, Portland, OR. AIAA paper 2004-2210, 2004.

[6] Russell M. Cummings, Carsten Liersch, and Andreas Schuette. "Multi-Disciplinary Design and Performance Assessment of Effective, Agile NATO Air Vehicles", 2018 Applied Aerodynamics Conference, AIAA AVIATION Forum, (AIAA 2018-2838) https://doi.org/10.2514/6.2018-2838

[7] Cummings, R.M. and Schuette A. et al., “Assessment of Stability and Control Prediction Methods for NATO Air and Sea Vehicles,” NATO RTO/AVT, Final Report of the AVT-161 Task Group, RTO-TR-AVT-161 AC/323(AVT-161)TP/440, Sept. 2012.

[8] Zimper, D.; Hummel, D.: Analysis of the transonic flow around a generic UCAV configuration. AIAA Paper 2014-2266, June 2014.

[9] Huber, K., Vicroy, D.D., Schütte, A., and Hübner, A.-R., ”UCAV model design investigations and static low speed wind tunnel experiments to estimate control device effectiveness and S&C capabilities,” AIAA-Paper 2014-2002, 32nd AIAA Applied Aerodynamics Conference, Atlanta, GA, 16-20 June, 2014.

[10] Galle, M., Gerhold, T., and Evans, J., “Technical Documentation of the DLR TAU-Code,” DLR-IB 233-97/A43, 1997.

[11] Allmaras, S.R., Johnson, F.T, and Spalart, P.R., “Modifications and Clarifications for the Implementation of the Spalart-Allmaras Turbulence Model,” Seventh International Conference on Computational Fluid Dynamics (ICCFD7), Big Island, Hawaii, 9-13 July 2012.

[12] Centaur Soft, “http://www.Centaursoft.com”

[13] Schütte, A.; Huber, K. C.; Zimper, D.: Numerische aerodynamische Analyse und Bewertung einer agilen und hoch gepfeilten Flugzeugkonfiguration. DGLR Paper-0001, Deutscher Luft- und Raumfahrtkongress, Rostock, 2015.

[14] Paul, M.; Rein, M.: Transonic Numerical and Experimental Investigation into Unconventional Lambda Wing Control Surfaces. AIAA Paper 2016-0799, Jan. 2016.

[15] Patrick Loechert, Kerstin C. Huber, Carsten Liersch, and Andreas Schuette. "Control Device Studies for Yaw Control without Vertical Tail Plane on a 53° Swept Flying Wing Configuration", 2018 Applied Aerodynamics Conference, AIAA AVIATION Forum, (AIAA 2018-3329) https://doi.org/10.2514/6.2018-3329

[16] Deere. K.A.: "Summary of fluidic thrust vectoring research conducted at NASA Langley Research Center``, AIAA paper 2003-2800, 2003.

[17] Mason, M. and Crowther, W., ``Fluidic Thrust Vectoring for Low Observable Air Vehicles", 2nd AIAA Flow Control Conference, Portland, OR. AIAA paper 2004-2210, 2004.

[18] Gal-Or B.: ``Fundamental Concepts of Vectored Propulsion". Journal of Propulsion Vol. 6, No.6, Nov - Dec 1990.

[19] Wilde, P., Crowther, W., Buonanno, A. and Savvaris, A.:``Aircraft Control Using Fluidic Maneuver Effectors", 26th AIAA Applied Aerodynamics Conference, AIAA paper 2008-6406, 2008.

[20] Anderson, C.J., Giuliano, V.J. and Wing, D.J.: ``Investigation of hybrid fluidic / mechanical thrust vectoring for fixed-exit exhaust nozzles", AIAA paper 97-3148, July 1997.

[21] Balu, R., Marathe, A.G., Paul P.J. and Mukunda, H.S.: ``Analysis of performance of a hot gas injection thrust vector control system", Journal of Propulsion and Power, Vol. 7, pp. 580–585, 1991.

[22] Deere, K.A., Flamm, J.D., Berrier, B.L. and Johnson, S.K.: ``Computational study of an axisymmetric dual throat fluidic thrust vectoring nozzle for a supersonic aircraft application", 43rd AIAA/ASME/SAE/ASEE Joint Propulsion Conference \& Exhibit, AIAA paper 2007-5085, 2007.

[23] Panitz, T. and Wasan, D.T.: ``Flow Attachment to Solid Surfaces: The Coanda Effect", AIChE Journal Vol. 18 No.1, pp 51-57, January 1972.

[24] Van der Veer M. and Strykowski P.J.: ``Counterflow Thrust Vector Control of Subsonic Jets: Continuous and Bistable Regimes", Journal of Propulsion and Power Vol. 13 No. 3, May-June 1997

[25] Flamm, J.D.: "Experimental study of a nozzle using fluidic counterflow for thrust vectoring", AIAA paper 98-3255, July 1998.